Topological lasing in resonant photonic structures

Laura Pilozzi* and Claudio Conti
Institute for Complex Systems, National Research Council (ISC-CNR), Via dei Taurini 19, 00185 Rome, Italy
(Received 19 February 2016; revised manuscript received 11 May 2016; published 27 May 2016)

We exploit topological edge states in resonant photonic crystals to attain strongly localized resonances and demonstrate lasing in these modes upon optical excitation. The use of virtually lossless topologically isolated edge states may lead to a class of thresholdless lasers operating without inversion. One needs, however, to understand whether topological states may be coupled to external radiation and act as active cavities. We study a two-level topological insulator and show that self-induced transparency pulses can directly excite edge states. We simulate laser emission by a suitably designed topological cavity and show that it can emit tunable radiation. For a configuration of sites following the off-diagonal Aubry-André-Harper model, we solve the Maxwell-Bloch equations in the time domain and provide a first-principles confirmation of topological lasers. Our results open the road to a class of light emitters with topological protection for applications ranging from low-cost energetically effective integrated laser sources, also including silicon photonics, to strong-coupling devices for studying ultrafast quantum processes with engineered vacuum.

DOI: 10.1103/PhysRevB.93.195317

I. INTRODUCTION

In the context of transport phenomena, two- or three-dimensional Bloch and Anderson models, paradigmatic for periodic and disordered structures, allow one to observe a crossover from extended to localized states [1] at a critical degree of disorder [2,3]. However, a different class of structures, i.e., the topological insulators, shows a localization phase transition [4] in one dimension (1D). Originally described in the tight-binding formulation for electrons [5,6], and recently for the study of localization properties of acoustic [7], electromagnetic [8–12], and matter waves [13], topological insulators are characterized by the presence of peculiar edge states, corresponding to a conducting surface for a bulk insulating material. The geometric phase of the bulk crystal determines the existence of these edge states and, correspondingly, they are protected, i.e., stable against any perturbation.

Recently, the study of localization properties in topological systems has been extended to the class of resonant photonic crystals [14,15] sustaining topologically protected boundary states [16], also involving the exciton-photon coupling [17]. The possibility of topologically protected states in resonant systems opens the challenge of realizing topologically sustained lasers, i.e., lasers based on edge states. These devices are expected to benefit from the intrinsic isolation, and hence may eventually operate at very low threshold or without population inversion. Indeed, the potential absence of loss reduces virtually to zero the gain needed for the laser operation.

In these terms, the first question to consider is whether resonant topologically isolated systems can be directly excited from external inputs and, seemingly, if topologically isolated states can emit coherent light into propagating modes when acting in a laser device.

In this paper, we show that a direct excitation of topological edge states is achievable in chains of two-level systems (TLS) by the use of an ultrashort self-induced transparency (SIT) pulse. By the Maxwell-Bloch equations [18,19], we study SIT in a resonant topological insulator (RTI) where index modulation is given by either the TLS or by the background dielectric function. In analogy with the disordered case [20], the spatial distribution of the active layers localizes the SIT pulse that would otherwise induce a traveling population inversion. This localization is a fingerprint for edge-state detection and sustain tunable laser emission.

II. STRUCTURE AND EDGE-STATE DISPERSION

A schematic of the system considered is shown in Fig. 1. The structured region consists of resonant two-level layers A (width L_A) in an homogenous bulk of frequency-independent dielectric function ε_b. Two configurations will be considered. In a uniform structure (US), the resonant layers, with their background dielectric function $\varepsilon_a = \varepsilon_b$, are arranged in a sequence with centers in $z_n = d_o[n + \eta d_n^H]$, where $d_n^H = \cos(2\pi\beta n + \phi)$ is the Harper modulation [6]. In a Bragg structure (BS), the resonant layers have $\varepsilon_a \neq \varepsilon_b$ and the widths b_n of the dielectric layers B are modulated as $b_n = b_o[1 + \eta d_n^H]$.

These distributions define a 1D bichromatic periodic lattice (period d_o) modulated by a secondary lattice with strength η. The phase shift ϕ governs the localization phase transition and the modulation frequency $2\pi\beta$ determines the number of topological boundary states in the gap. The structure is periodic with β^{-1} resonant layers in the unit cell and period $d = \beta^{-1}d_o$.

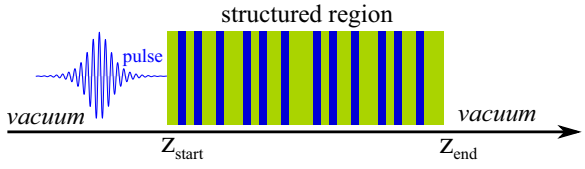

FIG. 1. Schematic view of the structured region: a 1D chain of resonant two-level layers (blue) in a homogeneous bulk (green) of frequency-independent dielectric function ε_b.

*Corresponding author: laura.pilozzi@isc.cnr.it

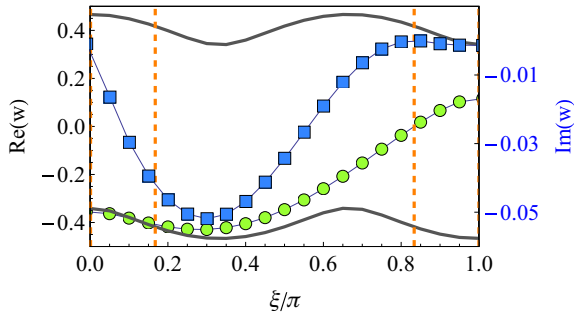

FIG. 2. Real (green circles) and imaginary (blue squares) part of the left-edge-state frequency for $\beta = 1/3$, $\eta = 0.2/\pi$, $\omega_o = 1.533$ eV, and $\varepsilon_b = 12.25$. The dashed vertical lines show the ξ values ($\xi/\pi = 0,1/6,5/6,1$) where, for symmetry reasons, edge states do not exist. The continuous lines mark the boundaries of the gap.

III. UNIFORM STRUCTURE

We choose $d_o = \lambda_o/2$ with $\lambda_o = 2\pi c/(\omega_o\sqrt{\varepsilon_b})$ in order to center the photonic band gap of the ordered stack ($\eta = 0$) at ω_o (TLS resonance). The A layers have radiative (nonradiative) Γ_o (Γ) decay rate, dielectric constant ϵ_a, and reflection coefficient $r_A(\omega) = -i/(w+i)$, with $w = (\omega - \omega_o + i\Gamma)/\Gamma_o$, with a local Lorentz-like dispersion,

$$\chi_A(\omega) = -\frac{\hbar^2 c^2}{\omega_o^2}\frac{L_A q^3}{16\pi}\frac{\left(q^2 L_A^2 - 4\pi^2\right)^2}{16\pi^4 \sin^2(qL_A/2)}\frac{1}{w}, \qquad (1)$$

with $q = \omega\sqrt{\epsilon_a}/c$. The poles of the reflection coefficient of the whole structure give the left-edge-state frequencies w_ℓ, i.e., solutions with negative imaginary part [16] of

$$e^{2iqs_1} + (w-i)^2 e^{2iq(s_1+s_2)} + (w+i)^2 + (w^2+1)e^{2iqs_2} = 0. \qquad (2)$$

The symmetry $w_r(\mp\xi) = w_\ell(\pm\xi)$, with $\xi = \phi - \pi/6$, gives the right-edge modes w_r. The states lay within the gap centered at ω_o with bounds given by $\mathrm{Tr}(T) = \pm 2$, where T is the single-period transfer matrix.

Figure 2 shows the ξ dependence of the real part (green circles) of the left-edge-state frequency. When ξ varies in $(0,\pi)$, the edge modes traverse the band gap, bounded by the straight lines; the imaginary part (blue squares) $\mathrm{Im}[(\omega - \omega_o + i\Gamma)/\Gamma_o]$ gives their inverse lifetime.

Figure 3 shows reflectivity intensity $|r_\infty(\xi,\omega)|^2$ [Fig. 3(a)] and phase [Fig. 3(c)] for $\Gamma_o = 10^{-2}\omega_o$ and $\Gamma = 10^{-2}\Gamma_o$ and the corresponding Chern numbers C. The reflection coefficient intensity allows one to locate allowed bands and gaps of the modulated ($\eta \neq 0$) structures, while the reflection coefficient phase allows one to deduce, from its winding numbers, the

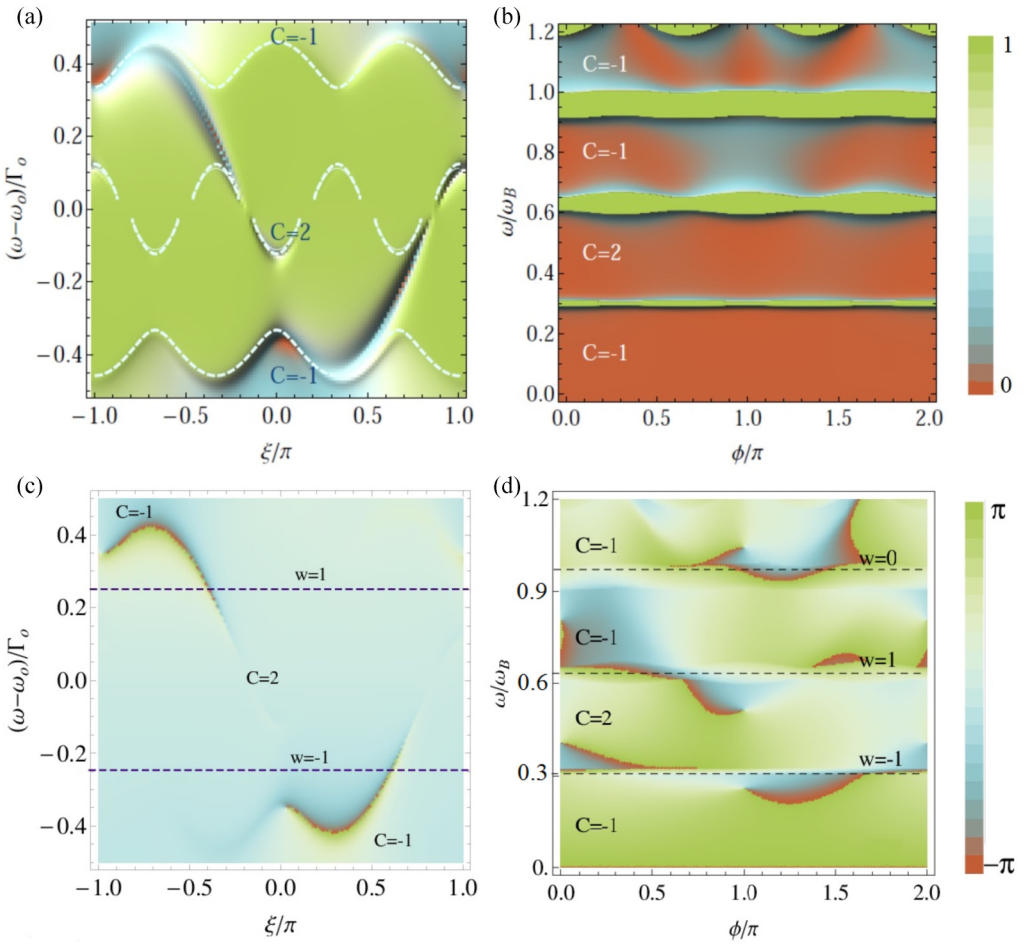

FIG. 3. Squared amplitude of the reflection coefficient $r_\infty(\phi,\omega)$ from the left side of the semi-infinite (a) US and (b) BS chain; reflection coefficient phase for the (c) US chain and (d) BS chain. Chern numbers C and winding numbers w are indicated.

topological invariants of the system under consideration. The allowed bands are indeed characterized by a Chern number given by the winding number of the reflection coefficient in the above-lying stop band minus that in the below-lying stop band [21].

The edge states correspond to dips in $|r_\infty(\xi,\omega)|^2$: their experimental observation requires fine spectral resolution and a high ratio between the radiative and nonradiative decay rates Γ_o/Γ. In these terms, 1D systems with weak losses and a large resonance strength Γ_o/ω_o are ideal candidates for edge-state detection.

IV. BRAGG STRUCTURE

For different dielectric constants of layers A and B, the spectral gaps of the structure with $\eta = 0$ at integer multiples of $\omega_B = \pi c/(L_a\sqrt{\varepsilon_a} + b_0\sqrt{\varepsilon_b})$ split in β^{-1} gaps. We choose $\varepsilon_a = 1$ and $\varepsilon_b = 12.25$, $b_0 = 200$ nm and $L_a = 48$ nm, so that $\omega_B = 0.828$ eV.

For $\beta = 1/3$ and $\eta = 0.5$, Fig. 3(b) shows the reflection coefficient $|r_\infty(\phi,\omega)|^2$ from the left edge of the semi-infinite system, while Fig. 3(d) shows the reflection coefficient phase. Chern numbers C of the allowed bands and winding numbers w of the gaps are shown [21]. Figure 4 shows the real [Fig. 4(a)] and imaginary [Fig. 4(b)] part of the left-edge eigenfrequencies, and the field intensity distribution [Fig. 4(c)] for $\phi = 0.7\pi$, with the localized mode profile at $\omega = \omega_{BS}(0.7\pi)$.

V. TIME-DOMAIN DYNAMICS

To obtain the electric-field amplitude, polarization, and population inversion, we describe the dynamics of light propagation in the RTI through the Maxwell-Bloch equations,

$$\mu_0\partial_t H_y = -\partial_z E_x, \quad \varepsilon_0\partial_t E_x = -\partial_z H_y - \partial_t P_x,$$

with $P_x = 2\gamma N\rho_1$, where N is the resonant dipole density and γ is the dipole coupling coefficient, and

$$\partial_t\begin{bmatrix}\rho_1\\ \rho_2\\ \delta\rho_3\end{bmatrix} = -\begin{pmatrix}\gamma_2 & -\omega_o & 0\\ \omega_o & \gamma_2 & -2\omega_R\\ 0 & 2\omega_R & \gamma_1\end{pmatrix}\begin{bmatrix}\rho_1\\ \rho_2\\ \delta\rho_3\end{bmatrix} + \begin{bmatrix}0\\ 2\omega_R\rho_{30}\\ 0\end{bmatrix}, \tag{3}$$

where $\delta\rho_3 = \rho_3 - \rho_{30}$, the vector $[\rho_1 \quad \rho_2 \quad \rho_3]^T$ is the state density vector, with ρ_1 (ρ_2) proportional to the in-phase (in-quadrature) polarization, ρ_3 proportional to the inversion population, and $\omega_R = \gamma E_x/\hbar$ the Rabi frequency; γ_1 and γ_2 denote the population and polarization relaxation rates, while ρ_{30} is the initial population inversion.

In the steady state and for a slowly varying field, for which $E_x = E_x^{eq} = \text{const}$, the Bloch equations give

$$\begin{aligned}\partial_t\rho_1^{eq} &= \omega_o\rho_2^{eq} = 0,\\ \partial_t\rho_2^{eq} &= -\omega_o\rho_1^{eq} + 2\tfrac{\gamma}{\hbar}E_x^{eq}\rho_3^{eq} = 0,\end{aligned} \tag{4}$$

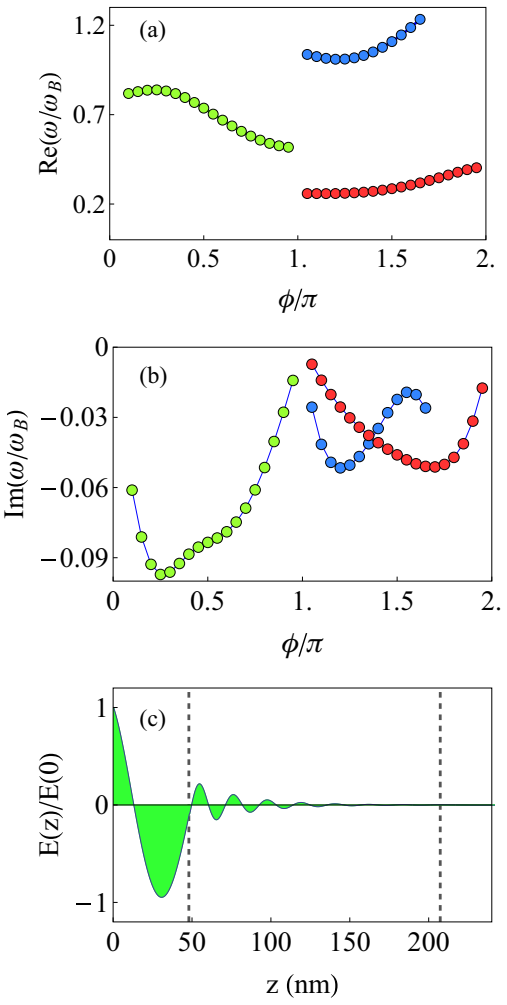

FIG. 4. (a) Real and (b) imaginary part of the left-edge-state frequency for $\beta = 1/3$, $\eta = 0.5$, $\varepsilon_a = 1$, and $\varepsilon_b = 12.25$. (c) Field intensity distribution inside the system for the configuration with $\phi = 0.7\pi$.

so that $\rho_2^{eq} = 0$ and $\rho_3^{eq} = \omega_o\rho_1^{eq}/(2\omega_R^{eq})$. Substituting $\rho_i(z,t) = \rho_i^{eq}(z) + \delta\rho_i(z,t)$ and neglecting fluctuations terms of order higher than one, we obtain the linearized equations around the steady state,

$$\begin{aligned}\partial_t\rho_1 &= -\gamma_2\rho_1 + \omega_o\rho_2,\\ \partial_t\rho_2 &= -\omega_o\rho_1 - \gamma_2\rho_2 - 2\gamma E_x/\hbar,\\ \partial_t\rho_3 &= -\gamma_1\rho_3,\end{aligned} \tag{5}$$

which, through a Fourier transform, allow us to define a susceptibility, $\chi(\omega) = -N\gamma\rho_1/(\varepsilon_o E_x)$, in the form

$$\chi(\omega) = \frac{2N\gamma^2}{\varepsilon_o\hbar}\frac{\omega_o}{(i\omega + \gamma_2)^2 + \omega_o^2}. \tag{6}$$

VI. SIT PULSE IN TOPOLOGICAL INSULATORS

Following Ref. [19], we consider the evolution of a pulse that coming from vacuum (ϵ_o) moves in the structured region of Fig. 1 with an initial sech profile: $E_x(0,t) = E_o\text{sech}[10(t-\tau/2)/(\tau/2)]\sin[2\pi f_o t]$. We choose the pulse frequency resonant with the medium, $2\pi f_o = \omega_o/\hbar$, the pulse

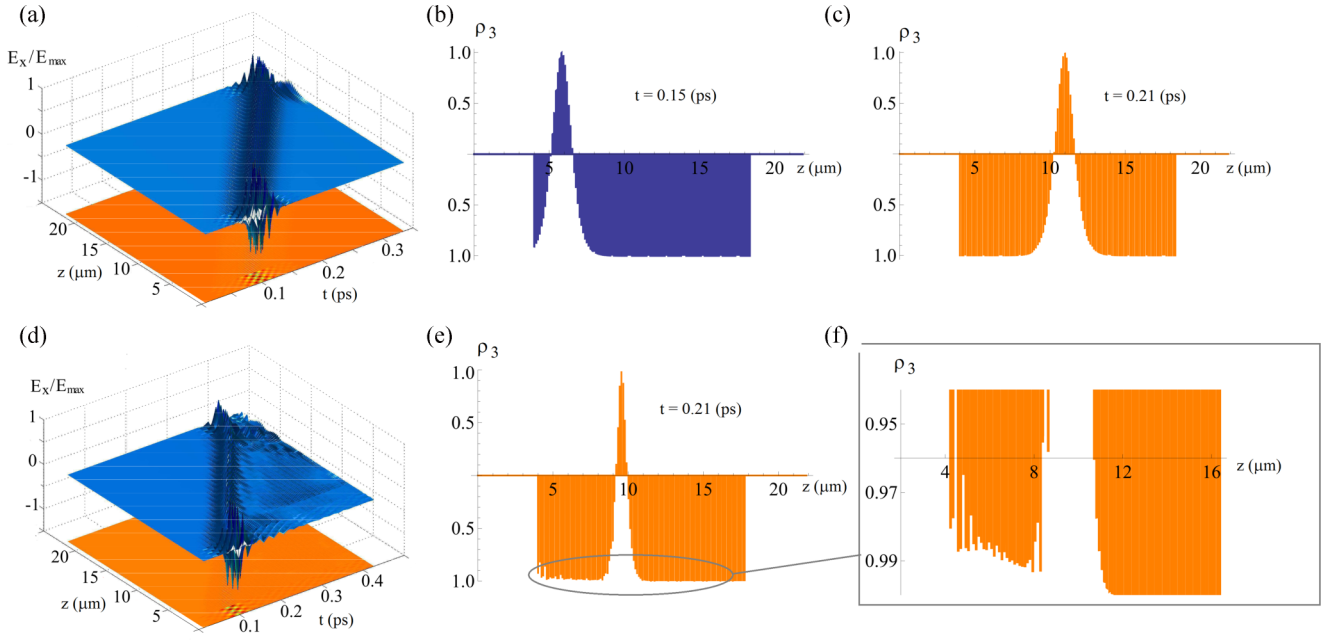

FIG. 5. Field and population inversion $\rho_3(z,t)$ spatial profile for different observation times t_i for the US structure with $\xi_{TC} = 0.5\pi$. (a)–(c) Reference configuration with $\gamma = 1 \times 10^{-29}$ Cm. (d)–(f) Topological configuration with $\gamma = 1.4 \times 10^{-27}$ Cm.

duration $\tau = 191$ fs, and E_o to have a 2π pulse [22] after the reflection on the input face due to the ϵ_o,ϵ_b mismatch. The one-dimensional periodic active medium consists of N_c cells with resonant layers L_A wide, separated by slices of transparent material with relative permittivity $\epsilon_b = 12.25$. The dielectric layers where the TLS are not present have $\rho_{30} = 0$ and widths $s_n = z_{n+1} - z_n - L_A$ for the US and $s_n = b_n$ for the BS. We model the US system as a collection of two-level atoms with density $N = 10^{24}$ m^{-3} and dipole coupling coefficient $\gamma = 1.4 \times 10^{-27}$ Cm, such that $N\gamma^2 = w\Gamma_o\chi_A(\omega_o)$. Moreover, we fix $\gamma_1 = \gamma_2 = 0.23$ THz. For the BS structure, we choose $N = 10^{24}$ m^{-3} and $\gamma = 1 \times 10^{-29}$ Cm.

We analyze the field and population inversion spatial profile for different observation times t_i. The $E_x(z,t)$ and $\rho_3(z,t)$ plots are shown in Fig. 5 for the US chain for which $N_c = 40$ and in Fig. 6 for the BS one for which $N_c = 50$. For both of the structures, $z_{\text{start}} = 4$ μm and a 2 μm layer of material ϵ_b is present at the front and rear side. To point out that the edge states are excited by the external input, we compare a topological configuration (TC) with a reference configuration (RC). In particular, according to the dispersion relations (Figs. 2 and 4), we choose

(i) for the US, $\xi_{TC} = 0.5\pi$, with an edge state at the frequency $\nu_\ell = 369.4$ THz and lifetime $\tau_\ell = 0.98$ ps; and

(ii) for the BS, $\phi_{TC} = 0.7\pi$, with an edge state at the frequency $\nu_\ell = 121.48$ THz and lifetime $\tau_\ell = 0.014$ ps.

The reference configuration is given by the choice $\epsilon_a = \epsilon_b$ for the BS chain. In the uniform one, we switch off the edge state by simply decreasing the dipole coupling coefficient. We remark that in the US, the modulation in the refractive index, given by the pulse interaction with matter, is the origin of both the gap and the edge state.

In the absence of an edge state [Fig. 5(a)], the incident laser pulse with its initial intensity and width evolves in a steady-state envelope and propagates without attenuation at a constant velocity. As a consequence, the maxima $\rho_3(z,t) = 1$, i.e., population inversion [Figs. 5(b) and 5(c)], track, in space and time, the same path for the excitation through the structure. The BS chain gives similar results.

On the contrary, in the topological configuration, the localization at the input face of the spectral component of the pulse corresponding to the edge-mode frequency is evident. For the US topological configuration, where the refractive index modulation is given only by the contribution of the resonance, the pulse propagates with a lower dispersion [Fig. 5(d)] with respect to the BS configuration [Fig. 6(a)]. In both cases, as a consequence of localization, the main pulse no longer meets the SIT condition and undergoes attenuation due to absorbtion by the TLS. The asymmetry in the $\rho_3(z,t)$ shape for the US chain, shown in Fig. 5(e), and in an enlarged scale in Fig. 5(f), is a fingerprint of this localization. The $\rho_3(z,t)$ shape in Fig. 6(b) for the BS chain shows attenuation of the main peak and evidence for the onset of the edge-mode propagation for times longer than its lifetime.

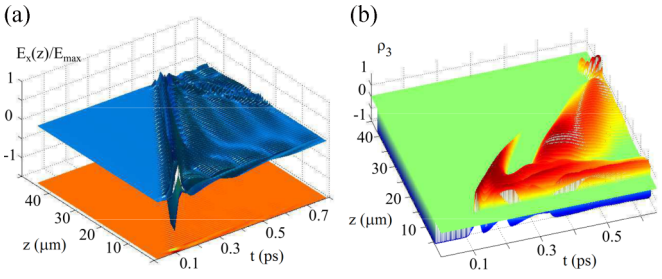

FIG. 6. (a) Field and (b) population inversion $\rho_3(x,t)$ spatial profile for different observation times t_i for the BS structure with $\phi_{TC} = 0.7\pi$.

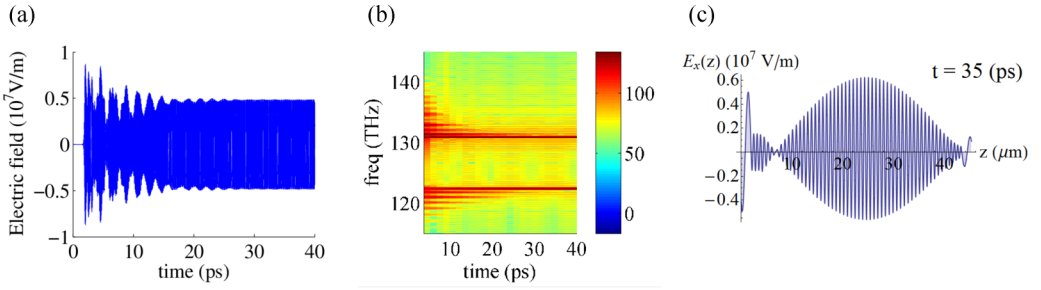

FIG. 7. (a) Time-dependent output intensity in the left side of the BS chain; mode beating is observed in the time range $(1 \div 30$ ps). (b) Time evolution of its spectrum. (c) Snapshot of the electric field for $t = 35$ ps.

VII. TOPOLOGICAL LASING

Our challenge is to show that the interplay of topological localization and amplification can be exploited to design mirrorless laser systems in analogy with random structures [23]. To this end, with the resonant layers as the light-amplifying material, we study edge modes in the stimulated emission process. We start with the two-level system population initially inverted in the upper state $\rho_{30} = 1$ and add, following Ref. [24], as the only source, a stochastic term with Gaussian statistic in the electric-field evolution $E_x = \sqrt{-2\xi_E \ln(a)}\cos(2\pi b)$, with a and b random numbers uniformly distributed in (0,1) interval and variance $\xi_E = 10^{-3}\,\mathrm{V}^2\,\mathrm{m}^{-2}$.

For the BS chain, with a gap in the range $(120 \div 134)$ THz, and $\phi = 0.7\pi$, the TLS resonance frequency is $\nu_o = \nu_\ell(0.7\pi)$. Other parameters are $\mathrm{N} = 10^{23}\,\mathrm{m}^{-3}$, $\gamma = 4.8 \times 10^{-28}$ Cm, $T_1 = 1/\gamma_1 = 10^{-11}$ s, and $T_2 = 1/\gamma_2 = 7 \times 10^{-15}$ s. For this system, Figs. 7(a) and 7(b) show the time-dependent output intensity in the left side of the structure, and the time-resolved spectrum. After a wide-band transient (t $\approx$ 1 ps), for $t \in (1 \div 30)$ ps, the emission is multimodal with a spectrum corresponding to delocalized Bloch modes at the photonic band gap (PBG) edges. At longer times ($t \gg 30$ ps), the high-quality factor modes survive and the spectrum is characterized by two main peaks: one at shorter wavelengths corresponding to the PBG lower edge and one inside the gap corresponding to the edge state $\lambda_\ell(0.7\pi) = 2469$ nm. This is confirmed by the electric-field spatial profile in Fig. 7(c) for $t = 35$ ps, which reveals the coexistence of a extended mode and a localization at $z \cong 4\ \mu$m.

The US chain provides similar results. From Eqs. (6) and (1), for given N and Γ_o, the dipole coupling coefficient is fixed by $N\gamma^2 = w\Gamma_o\chi_A(\omega_o)$. On the other hand, the Γ_o value allows one to control the gap width $\Delta\omega = 2w_U\Gamma_o$ and the left-edge-mode resonance $\omega_\ell = w_L\Gamma_o + \omega_o$. This circumstance allows a tunable field emission, either varying Γ_0 or the pumping rate N. We choose $\xi = 0.5\pi$, furnishing $w = w_U = 0.4179$ and $w = w_L = -0.3465$ for the stop band upper edge and left-edge mode in Fig. 2.

As shown in Fig. 8(a) for $\mathrm{N} = 10^{23}\,\mathrm{m}^{-3}$ and $\Gamma_o = 5.89 \times 10^{-3}$ eV, stimulated emission starts to overtake the spontaneous one after a transient regime (t $\approx$ 3 ps) of laser field buildup. Once the steady state is reached, the spectrogram of the emitted signal shows characteristic peaks. The peak at $\nu \approx 385$ THz corresponds to a delocalized mode. In addition, the optical feedback edge-mode localization gives rise to emission at $\nu_\ell = 370.2$ THz. For this system, a wavelength

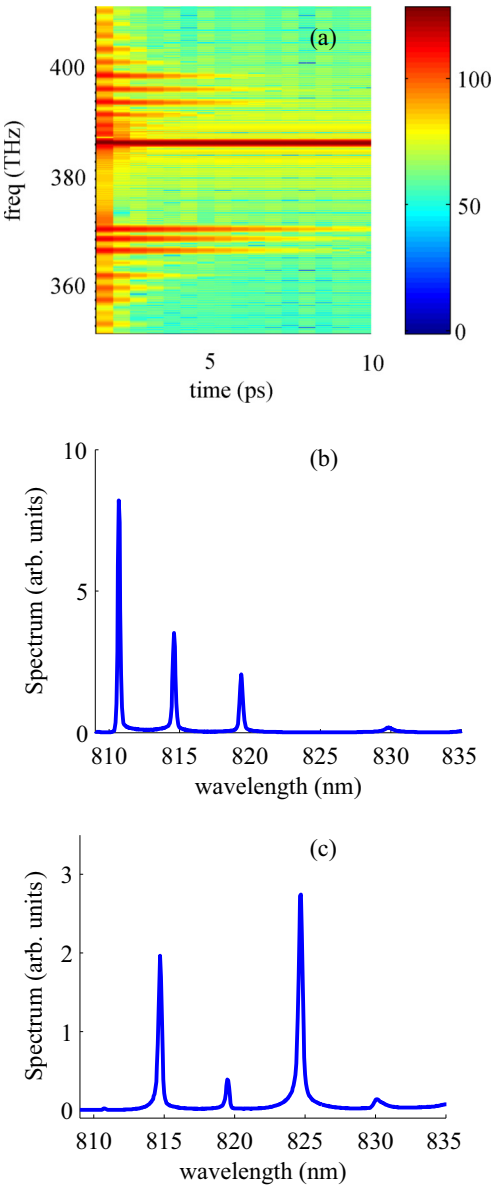

FIG. 8. (a) Time-dependent spectrum of the output signal in the left side of the US chain. Emitted spectrum for (b) $\Gamma_o = 5.89 \times 10^{-3}$ eV and (c) $\Gamma_o = 2.945 \times 10^{-2}$ eV.

tuning of the emitted spectrum can be obtained, changing the Γ_o value as shown in Fig. 8(b) for $\Gamma_o = 5.89 \times 10^{-3}$ eV where $\lambda_\ell = 810.2$ nm, and in Fig. 8(c) for $\Gamma_o = 2.945 \times 10^{-2}$ eV where $\lambda_\ell = 814$ nm.

One of the main advantages of topological protection and intrinsic isolation of the edge states is to lower the threshold for laser action. This is achieved by loss reduction and high gain efficiency due to limited emission bandwidth of the active medium. In our calculation, this is reflected in a reduction of the two-level atoms' density $N = 10^{23}\,\mathrm{m}^{-3}$ to achieve lasing in the topological configuration with respect to an equivalent periodic array for which $N = 10^{24}\,\mathrm{m}^{-3}$, corresponding to one order of magnitude reduction in the laser threshold.

VIII. CONCLUSIONS

In this paper, we have analyzed the time-resolved optical response to an ultrashort light pulse and focused on edge-state detection in 1D resonant topological insulators given by two-level layers in uniform and modulated refractive index structures. For favorable system parameters obtained through linearized Maxwell-Bloch equations, we show that a direct observation of topological protected edge states can be achieved following the time evolution of the population inversion with different properties of uniform structures with respect to periodic systems. We provide evidence that a RTI can act as a resonator with laserlike emissions due to localized edge modes; we also show that the emission frequency can be tuned by acting on the pumping energy or other system parameters.

An experimental test of our results is possible by the use of active TLS of quantum wells embedded in a semiconductor structure with periodically alternating linear index of refraction. For these systems, the mechanism of emission is expected to have a low or vanishing laser threshold since, being the resonator directly etched in the amplifying material, an effective feedback can be obtained.

The use of topologically protected states for lasing in resonant systems may open a variety of several new directions in laser physics. Achieving laserlike action may be favored in regimes in which no feasible way for inversion population can be imagined as, for example, for silicon lasers; in addition topologically protected states may also allow very narrow band emission because of the low coupling with radiation modes, proving extremely coherent sources at room temperature for metrological and spectroscopic applications.

ACKNOWLEDGMENTS

We acknowledge support from the ERC project VANGUARD (Grant No. 664782) and the Templeton Foundation (Grant No. 58277).

[1] P. W. Anderson, Phys. Rev. **109**, 1492 (1958).
[2] K. Ishii, Prog. Theor. Phys. Suppl. **53**, 77 (1973).
[3] D. J. Thouless, Phys. Rep. **13**, 93 (1974).
[4] M. Verbin, O. Zilberberg, Y. E. Kraus, Y. Lahini and Y. Silberberg, Phys. Rev. Lett. **110**, 076403 (2013).
[5] S. Aubry and G. André, Ann. Israel. Phys. Soc. **3**, 133 (1980).
[6] P. G. Harper, Proc. Phys. Soc. London Sect. A **68**, 874 (1955).
[7] Zhaoju Yang, Fei Gao, Xihang Shi, Xiao Lin, Zhen Gao, Yidong Chong, and Baile Zhang, Phys. Rev. Lett. **114**, 114301 (2015).
[8] Z. Wang, Y. Chong, J. D. Joannopoulos, and M. Soljacic, Nature (London) **461**, 772 (2009).
[9] M. C. Rechtsman, J. M. Zeuner, Y. Plotnik, Y. Lumer, D. Podolsky, F. Dreisow, S. Nolte, M. Segev, and A. Szamei, Nature (London) **496**, 196 (2013).
[10] L. Lu, J. D. Joannopoulos, and M. Soljacic, Nat. Photon. **8**, 821 (2014).
[11] Y. E. Kraus, Y. Lahini, Z. Ringel, M. Verbin, and O. Zilberberg, Phys. Rev. Lett. **109**, 106402 (2012).
[12] S. Ganeshan, K. Sun, and S. Das Sarma, Phys. Rev. Lett. **110**, 180403 (2013).
[13] G. Roati, C. D'Errico, L. Fallani, M. Fattori, C. Fort, M. Zaccanti, G. Modugno, M. Modugno, and M. Inguscio, Nature (London) **453**, 895 (2008).
[14] A. N. Poddubny, L. Pilozzi, M. M. Voronov, and E. L. Ivchenko, Phys. Rev. B **77**, 113306 (2008).
[15] A. N. Poddubny, L. Pilozzi, M. M. Voronov, and E. L. Ivchenko, Phys. Rev. B **80**, 115314 (2009).
[16] A. V. Poshakinskiy, A. N. Poddubny, L. Pilozzi, and E. L. Ivchenko, Phys. Rev. Lett. **112**, 107403 (2014).
[17] T. Karzig, C.-E. Bardyn, N. H. Lindner, and G. Refael, Phys. Rev. X **5**, 031001 (2015).
[18] A. Taflove and S. C. Hagness, *Computational Electrodynamics: The Finite-Difference Time-Domain Method* (Artech House, Boston, 2005).
[19] Richard W. Ziolkowski, John M. Arnold, and Daniel M. Gogny, Phys. Rev. A **52**, 3082 (1995).
[20] V. Folli and C. Conti, J. Opt. Soc. Am. B **29**, 2080 (2012).
[21] A. V. Poshakinskiy, A. N. Poddubny, and M. Hafezi, Phys. Rev. A **91**, 043830 (2015).
[22] S. L. McCall and E. L. Hahn, Phys. Rev. Lett. **18**, 908 (1967).
[23] C. Conti and A. Fratalocchi, Nat. Phys. **4**, 794 (2008).
[24] G. Slavcheva, J. Arnold, and R. Ziolkowski, IEEE J. Sel. Top. Quantum Electron. **10**, 1052 (2004).